



LJMU Research Online

Rowe, WB

Conical hydrostatic journal bearings for high speeds

<http://researchonline.ljmu.ac.uk/id/eprint/13092/>

Article

Citation (please note it is advisable to refer to the publisher's version if you intend to cite from this work)

Rowe, WB (2020) Conical hydrostatic journal bearings for high speeds. Proceedings of the Institution of Mechanical Engineers, Part J: Journal of Engineering Tribology. ISSN 1350-6501

LJMU has developed **LJMU Research Online** for users to access the research output of the University more effectively. Copyright © and Moral Rights for the papers on this site are retained by the individual authors and/or other copyright owners. Users may download and/or print one copy of any article(s) in LJMU Research Online to facilitate their private study or for non-commercial research. You may not engage in further distribution of the material or use it for any profit-making activities or any commercial gain.

The version presented here may differ from the published version or from the version of the record. Please see the repository URL above for details on accessing the published version and note that access may require a subscription.

For more information please contact researchonline@ljmu.ac.uk

<http://researchonline.ljmu.ac.uk/>

1. Original research article

2. Corresponding author info

Corresponding Author:

Professor W Brian Rowe, DSc, FIMechE, Court Cottage,
Moult Hill, Salcombe, TQ88LF, UK.

Email: browe1@btinternet.com

3. Conical Hydrostatic Journal Bearings for High Speeds

4. Author

Professor W Brian Rowe, DSc, FIMechE, Court Cottage,
Moult Hill, Salcombe, TQ88LF, UK.

5. Abstract

Conventional conical hydrostatic bearings are compared with less conventional three-recess and four-recess designs for operation in hybrid hydrostatic/hydrodynamic mode. Design implications are discussed with reference to operation at either low or high speeds. Conical spindle bearings are chosen for this study because they offer a compact arrangement that allows both radial load support and axial load support. While there is wide availability of design data for separate thrust and cylindrical journal bearings there is very little data for conical bearings. This paper reviews the design of conical bearings and extends from previous knowledge into hybrid performance at high speeds. It is shown that long narrow recesses larger radial load support compared to long wide recesses for higher speeds.

Sample data are provided for design of single cone bearings and also for opposed cone bearings. The data provide for radial and axial loads applied in combination for a selection of cone angles. Data are also provided as a guide for flowrate in the concentric bearing state and for effects on temperature rise.

Keywords Hydrostatic, Hydrodynamic, Hybrid, Journal Bearings, High Speed, Conical, Design

6. Declaration

The author has received no funding for this research and has received no assistance in the conduct or in the preparation of this research article.

Conical Hydrostatic Journal Bearings for High Speeds

W Brian Rowe

Abstract

Conventional conical hydrostatic bearings are compared with less conventional three-recess and four-recess designs for operation in hybrid hydrostatic/hydrodynamic mode. Design implications are discussed with reference to operation at either low or high speeds. Conical spindle bearings are chosen for this study because they offer a compact arrangement that allows both radial load support and axial load support. While there is wide availability of design data for separate thrust and cylindrical journal bearings there is very little data for conical bearings. This paper reviews the design of conical bearings and extends from previous knowledge into hybrid performance at high speeds. It is shown that long narrow recesses offer larger radial load support compared to long wide recesses for higher speeds.

Sample data are provided for design of single cone bearings and also for opposed cone bearings. The data provide for radial and axial loads applied in combination for a selection of cone angles. Data are also provided as a guide for flowrate in the concentric bearing state and for effects on temperature rise.

Keywords: Hydrostatic, Hydrodynamic, Hybrid, High speed, Journal Bearings, Conical, Design

1 INTRODUCTION

Conical hydrostatic journal bearings can be employed for thrust bearings or for spindle bearings arrangements. Conical arrangements have advantages compared with separate journal and thrust bearings. Only two bearings are required for conical designs compared with two journal bearings and two thrust bearings for separate arrangements. This makes for economy of flow, economy of power and fewer parts. Furthermore, clearance is adjustable on assembly by adjustment of the axial location. However, accurate machining and accurate assembly of conical designs are required to ensure bearing alignment. The recesses for conical designs are relatively simple to manufacture by electro-discharge machining using a graphite carbon electrode suitably shaped that can be advanced axially into the bearing cones.

For brevity, the following research review is limited to publications on conical hydrostatic journal bearings, since there are hundreds of papers on other hydrostatic bearings

Conical spindle bearings were applied by the author in 1967 for a precision grinding spindle used in an optical profile grinding machine, [1-2]. The spindle operated at 7000 rev/min and was remarkable for its smooth running and precision grinding performance. Approximate load and flow equations for hydrostatic conical bearings were published by Stansfield in 1970, [3]. Aston et al, 1970 and 1971, computed load and flow using the lumped parameter technique, [4-5]. Ettles and Svoboda in 1975 investigated a double conical bearing for high speeds and commented on geometrical constraints limiting the cone angles that could be employed, [6]. This unconventional design was basically a hydrodynamic conical bearing although a degree of external pressurization was introduced to overcome insufficient radial load support. Rowe

in 1983, provided design procedures for hydrostatic conical bearings based on design maps derived for axial and radial loads applied in combination, [7]. Sharma et al in 2011 provided results for capillary compensated conical hydrostatic bearings [8]. Rowe in 2012, extended the design data in reference [7] using finite difference (FD) computer solutions for greater accuracy and range of application. Data and design procedures were made available for both hydrostatic and aerostatic conical bearings including complementary cone arrangements, [9]. Zuo et al in 2013, published a new design of conical hydrostatic journal bearing where in-built restrictor lands introduce self-compensation, [10]. It offers benefits of increased radial stiffness but introduces further complexity into the mechanical structure. Khakse et al in 2016 analysed non-recessed hydrostatic conical journals with hole entry, having either capillary or orifice restrictors, [11]. The load performance was compared with and shown to be very similar to non-recessed slot entry cylindrical plain bearings as described in ref [9]. The unified design approach used for definition of the speed domain in reference [7] was confirmed by Bassani and Piccigallo in 1992, and gave comparable results for hybrid cylindrical plain bearings, [12]. The design data for the conical hydrostatic bearings up to this point ignore hydrodynamic lift at high speeds. In practice, load support can be greatly increased as shown for cylindrical journals by taking advantage of hydrodynamic forces, [9-12]. The extra lift provides additional safeguard for radial overload and offers an increased range of application. This study advances previous work by exploring combined hydrostatic and hydrodynamic load support at high speeds, employing either four recesses or three recesses to maximize plain bearing land area where it is most useful. It is shown that long and narrow or thin-recess bearings offer excellent hybrid load performance compared with wide-recess bearings and also offer strong scavenging flow to offset hot spot generation. Optimization procedures allow hybrid loads to be maximized and make it possible to critically assess safe operating regions.

2 BEARING ARRANGEMENTS

Bearing configurations are compared in Figures 1(a) and (b). The conventional conical hydrostatic bearing with four wide recesses is shown in Figure 1(a). The proposed bearing with three narrow recesses is shown in Figure 1(b). Both types of bearing carry applied loads by means of an external pump and a constant supply pressure P_s . The conventional bearing is optimized for hydrostatic load support based on P_s . By contrast, the thick-land thin-recess conical bearing is designed to support substantial additional loads generated by hydrodynamic action at high speeds. In both designs, provision is made for separate supply through an individual flow restrictor for each recess. The restrictors may be capillary, orifice, or slot restrictors. Another possibility is that a separate constant flow supply is ensured for each recess. For the data calculated in this paper, it is assumed that laminar flow restrictors are employed such as capillaries or slots.

The design and operation of basic cylindrical hydrostatic bearings is well understood and Rowe 2012 provides detailed information on many aspects. The purpose of this paper is to establish basic principles and data for conical hybrid journal bearings operating at low to high speeds. It is also shown that a 4-recess bearing designed with long thin recesses offers hybrid performance almost as good as the 3-recess bearing with long thin recesses. Both designs offer much better load support than a conventional wide recess bearing.

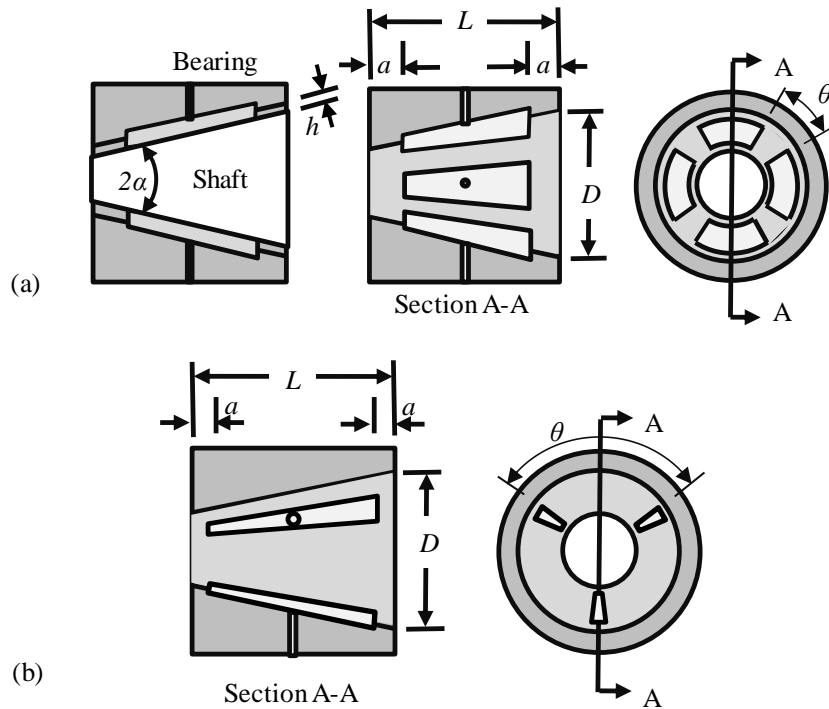


Figure 1. (a) A conventional 4-recess conical hydrostatic bearing with wide recesses [Rowe 2012]. (b) A 3-recess conical hydrostatic bearing with long thin recesses.

The long thin recesses shown in Figure 1(b) lead to wide inter-recess lands. The wide inter-recess lands allow substantial hydrodynamic pressures to be generated. Another advantage, is that the long thin recesses allow cooling flow to be distributed along the length of the bearing. Possible configurations for opposed pad complementary-cone arrangements are illustrated in Figure 2. The two conical bearings at each end of the spindle should be well separated as shown rather than closely spaced. Close spacing is not recommended as explained more fully by Rowe 2012. Wide spacing allows either central application of radial loads or, as more usual, overhung application of radial loads. The advantage of a widely spaced arrangement is that a slight tilt allows the total radial load supported to be almost doubled. With closely spaced bearings a slight tilt greatly reduces minimum film thickness. Initial alignment during manufacture is also simplified with widely spaced arrangements.

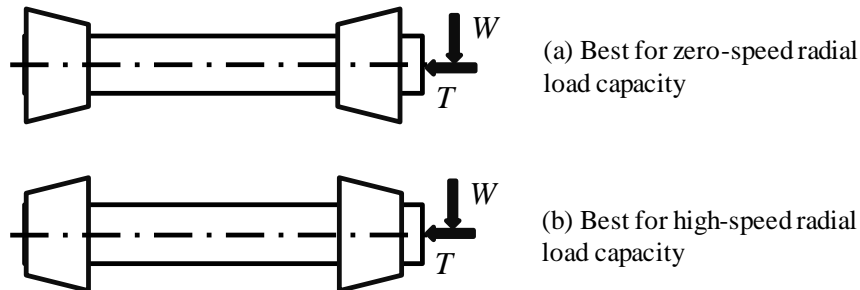


Figure 2. Alternative arrangements for overhung loads

Data are given below for a single cone while progressing development of suitable parameters for hybrid operation. Subsequent data are given for opposed pad bearings. Data are given for the maximum radial load that can be supported on one bearing while the maximum thrust load

is for the opposed pair acting together. The designer must first specify the maximum radial and thrust reaction loads and then evaluate the radial reaction forces on each bearing. Specified radial and thrust loads must not be exceeded. Exceeding the specified thrust load reduces the radial load that can be supported and also reduces the minimum film thickness.

If axial thrust loads applied to the journal are very small in comparison with radial loads, a small cone angle is best. However, if applied thrust loads are large, it may be necessary to design for a larger cone angle. Data are provided for four cone angles covering a suitable range. It is considered that a semi-cone angle of 15° is large enough to satisfy most situations.

This paper documents the development of suitable hybrid conical bearings. It also provides computed data for supported loads. Four-recess bearings are compared with three-recess bearings for hybrid performance over a range of zero, moderate and high speeds.

3 SYMBOLS AND DESIGN PARAMETERS

3.1 Geometry and Fluid Properties

D	Bearing diameter at large end of cone
D_j	Bearing diameter at intermediate position along length
L	Axial bearing length
U	Journal surface speed
N	Journal rotational speed
P_s	Constant supply pressure
Q_f	Dimensionless flow factor defined below
T	Axial applied load on pair of opposed bearings
ΔT	Adiabatic temperature-rise for single pass of liquid
W	Radial applied load on one bearing
A_f	Total effective bearing friction area
a	Axial land width
h_o	Concentric film thickness normal to bearing surface
h	Normal film thickness
h_r , and h_{ro}	Radial film thickness and concentric radial film thickness
h_a , and h_{ao}	Axial film thickness and concentric axial film thickness
n	Number of recesses around bearing
p_r	Recess pressure
$a \sec \alpha$:	Land width measured along cone surface
x, z	Circumferential and longitudinal bearing coordinates
α	Semi-angle of cone
β :	Recess pressure/supply pressure when the journal is concentric
ϵ :	Radial eccentricity ratio
θ :	Included angle of inter-recess land
ϕ :	Angle of eccentricity from mid inter-recess land
η :	Dynamic viscosity of the fluid
ψ :	Attitude angle between W and ϵ

3.2 Parameters Used for Computation and Data Presentation

$\bar{A}_f = A_f/D^2$ Dimensionless friction area

$\beta = p_{ro}/P_s$	Concentric pressure ratio
$P_r = p_r/P_s$	Pressure ratio
$q = \frac{\beta P_s h_0^3 D}{\eta a} \cdot Q_f$	Hydrostatic flow q and dimensionless flow Q_f
$\bar{Q}_f = Q_f D/a$	Further dimensionless flow factor
$W = P_s L D \cdot \bar{W}$	Radial load support
$T = P_s D^2 \cdot \bar{T}$	Axial load support
$D_j = D \cdot \bar{D}_j$	Journal diameter
$L_1 = L \cdot \sec \alpha$	Length along journal surface
$h = h_0 \cdot H$	Film thickness h and dimensionless thickness H
$p = P_s \cdot P$	Pressure p and dimensionless pressure P
$S_h = \frac{\eta N}{P_s} \left(\frac{D}{2h_0} \right)^2$	Speed parameter
$K = \frac{H_f}{H_p} = \frac{\eta^2 A_f U^2}{P_s^2 \cdot Q_f \cdot h_0^4}$	Power ratio = friction power / pumping power
$\bar{X} = h_a/h_{ao}$	Axial position ratio
$1 - \bar{X}$	Axial displacement ratio
$\epsilon = e_r/h_{ro}$	Radial eccentricity ratio
a/L	Axial landwidth ratio (0.1 or 0.25)
$G = \frac{L_1 n_g}{D m \pi}$	Shape factor for grid element

4 THEORETICAL ANALYSIS

4.1 Finite Difference Solution of the Pressure Field

The basic equations for hydrostatic lubrication are well known and established. For this paper it is therefore only necessary to give a brief description of the basic theory and computational stages involved. A form of the Reynolds equation for steady loading of the fluid bearing film allowing for varying diameter and speed along the length is:

$$\frac{\partial}{\partial x} \left(\frac{\rho h^3}{12\eta} \frac{\partial p}{\partial x} \right) + \frac{\partial}{\partial z} \left(\frac{\rho h^3}{12\eta} \frac{\partial p}{\partial z} \right) = \frac{\rho \pi D_j N}{2} \frac{dh}{dx} \quad (1)$$

In parallel with solution of the bearing film pressures, it is necessary to solve the recess pressures. A finite difference (FD) technique was employed to solve the Reynolds equation, first solving the concentric film pressures using the concentric recess pressures as the internal boundary condition. Typically, a 150 x 40 FD grid was employed, denominating position nodes $i = 1$ to $n_g = 150$ around the circumference and $j = 1$ to $m = 40$ along the length.

The FD equation employed for solution of the bearing film pressures has the form:

$$P_{i,j} = \left\{ \frac{G}{\bar{D}_j} [H_{i+1/2}^3 P_{i+1,j} + H_{i-1/2}^3 P_{i-1,j}] + \frac{\bar{D}_j H_i^3}{G^2} [\bar{D}_{j-1/2} P_{i,j-1} + \bar{D}_{j+1/2} P_{i,j+1}] - 24 \frac{\pi L_1}{m D} S_h \bar{D}_j [H_{i-1/2} - H_{i+1/2}] \right\} / \left\{ \frac{G}{\bar{D}_j} [H_{i+1/2}^3 + H_{i-1/2}^3] + 2 \frac{\bar{D}_j^2}{G^2} H_i^3 \right\} \quad (2)$$

At high speeds and radial eccentricity ratios, hydrodynamic bearings cavitate. This is the situation where bearing pressures in the diverging film region initially become negative and then with further eccentricity the negative fluid film stresses collapse back to zero as the fluid film ruptures. This situation is accommodated in the computation using the usual approximation where negative pressures are set to zero.

After successive iterations of the pressure field, convergence is achieved. From the derived pressures, it is possible to sum the bearing flows through the whole bearing and also through each restrictor and recess.

The recess inlet pressures depend both on the resistance characteristics of the flow restrictors and the bearing film flow resistances from each recess. The subject of flow restrictors is fully described in Chapter 5 of Rowe 2012, [9]. For the purpose of solving the conical bearing, the subject can be understood as follows. The flow out from each recess must equal the flow in through the appropriate restrictor. The flow from the r^{th} recess may be calculated by summing the individual dimensionless flows \bar{q}_k to the nodes surrounding the recess adding appropriate pressure terms and speed terms at each node where, $\bar{q}_r = \sum \bar{q}_k = \sum \eta q_k / P_s h_0^3$.

Flow summation performed for the concentric shaft yields a value \bar{q}_{r0} . The flow through a capillary restrictor for the concentric condition is given by

$$\bar{q}_{r0} = (1 - P_r) / (k_c h_0^3) \quad (3)$$

The capillary factor $k_c = \pi d_c^4 / 128 l_c$ is a constant.

Flow summation from the r^{th} recess performed for the eccentric shaft yields a value \bar{q}_r and hence:

$$\frac{\bar{q}_r}{\bar{q}_{r0}} = \frac{1 - P_r}{1 - \beta} \quad (4)$$

During the iteration process, new values of recess pressure can therefore be derived with some manipulation by substituting the FD expression for \bar{q}_r into:

$$P_r = 1 - (1 - \beta) \bar{q}_r / \bar{q}_{r0} \quad (5)$$

Successive iterations of film pressures and recess pressures leads to a stable convergence of the pressure, load and flow parameters until sufficient accuracy is achieved. Better than 0.1% is usually considered satisfactory. Following convergence of the pressure field, bearing flows and reaction forces are summed in the usual way.

4.2 Axial Displacement Ratio and Radial Eccentricity Ratio

Radial eccentricity ratio is $\epsilon = e_r / h_{r0}$. Axial film thickness is $\bar{X} = h_a / h_{a0}$ so that axial displacement ratio is $1 - \bar{X}$. Minimum film thickness is $h_{min} = (1 - \epsilon) \bar{X} h_0$. The shaft is assumed to be displaced to a fixed eccentric position. The radial direction of the line of eccentricity is directed towards a mid-recess position when $\phi = 0$.

When axial and radial loads are employed together, it is advisable to base design values conservatively, particularly for the cone having reduced film thickness. Axial displacement ratio of 0.2 for a complementary cone arrangement gives film thickness values of $\bar{X} = 0.8$ and 1.2. Combining $\epsilon = 0.5$ and $\bar{X} = 0.8$ reduces minimum film thickness to $0.4h_0$. A more heavily loaded combination would be $\epsilon = 0.7$ and $\bar{X} = 0.8$ resulting in a minimum film thickness of $0.24h_0$. These maximum radial and axial displacements should not be exceeded for zero-speed hydrostatic operation without great caution although, with caution, slightly increased displacements may be permissible in high-speed hybrid operation.

4.3 Concentric Pressure Ratio

Restrictors for hydrostatic bearings are generally designed so that concentric pressure ratio $\beta = 0.5$. It should be noted that the effective concentric pressure ratio changes when an axial displacement is imposed corresponding to a new value of film thickness \bar{X} . The relaxation procedure is performed to solve for effective recess pressures and film pressures for the axially displaced shaft. Since the bearing arrangement is to be solved for opposed pads, an effective concentric pressure ratio β_h must be calculated for the heavily loaded pad and an effective concentric pressure ratio β_l for the lightly loaded bearing pad. The effective concentric pressure ratios for axially displaced pads are given by the well-established equation for hydrostatic thrust pads [8].

$$\beta_{eff} = 1 / \left[1 + \frac{1-\beta}{\beta} \cdot \bar{X}^3 \right] \quad (6)$$

Large variations from $\beta = 0.5$ leads to unacceptable pressure ratios after applying an axial displacement. Axial film thickness $\bar{X} = 0.75$ modifies concentric pressure ratio from $\beta = 0.5$ to effective values of $\beta_e = 0.7$ and $\beta_e = 0.34$ for the smaller gap bearing and the larger gap bearing respectively. This combination allows reasonable load support in both cones and is judged acceptable. For hydrostatic bearings, $\beta = 0.5$ is the suggested concentric pressure ratio value for complementary cone arrangements.

4.4 Power Ratio and Speed Parameter

It is not always realized that power ratio is a great simplification in bearing design allowing selection of suitable combinations of design variables such as speed, viscosity, clearance and landwidth ratio. It was shown by Opitz 1967, that the minimum power when varying viscosity for a particular speed is obtained when the power ratio $K = 1$, [13]. Alternatively, when varying concentric clearance, minimum power is obtained when $K = 3$. These two values are limits for purely hydrostatic bearings so that it is possible to specify an optimum range $1 \leq K \leq 3$. The power ratio is a unique characterization of the speed domain of a hybrid bearing as should be clear from the following discussion of results. The speed characteristics of hybrid bearings are uniquely defined by the power ratio. In the power ratio range 1-3, a hybrid bearing is always in the range 'low-speed' to 'moderate-speed'. The power ratio range 9-12 is always 'high-speed'. Power ratios in the 25-50 range are 'very high-speed'.

Power ratio K is closely related to the widely-employed speed parameter S_h . The speed parameter for optimum power ratio $K = 1$ is usually termed S_{h0} . Power ratio is proportional to speed squared so that $K \propto N^2 \propto S_h^2$. This means increasing K from 1 to 3, corresponds to increasing speed by nine times.

Running at speeds within the optimum range for hydrostatic operation yields increased bearing load support as seen in the results that follow. However, deliberately designing the bearing geometry for increased hydrodynamic load support and at the same time further increasing the power ratio reduces hydrostatic load support but increases total load support. Increasing the power ratio from $K = 1$ to $K = 12$ implies increasing the speed by 144 times and the speed parameter $S_h = 144S_{h0}$.

For a particular bearing geometry and concentric pressure ratio, an expression for concentric speed parameter can be determined from the parameter definitions given in 3.2 above [9]:

$$S_h = \frac{1}{4\pi} \sqrt{K\beta\bar{Q}_f/\bar{A}_f} \quad (7)$$

Equation (7) is a convenient form for calculating required numerical values for S_h having first selected a bearing geometry and a suitable value of K .

4.5 Adiabatic Temperature Rise

At zero speed, the adiabatic temperature rise of a liquid bearing lubricant can be found by assuming pressure energy is all converted into heat. The temperature rise depends on the supply pressure P_s , the heat capacity c of the liquid and the density ρ of the liquid. The term for flowrate cancels in the two expressions for pressure energy and the enthalpy rise so that:

$$\Delta T = P_s / c\rho \quad (8)$$

Temperature rises with time if the heated lubricant is allowed to re-enter bearing. Temperature rise with time can be prevented by cooling the lubricant in a cooler. Temperature rise can also be reduced if the liquid is cooled after passing through the restrictors and before passing through the bearing.

At speed, the heat energy is increased by frictional heating as the liquid passes through the bearing. The total temperature rise including the effect of supply pressure and frictional heating for a single pass through the bearing can be estimated very conveniently based on the power ratio K :

$$\Delta T = P_s(1 + K) / c\rho \quad (9)$$

For a typical zero speed bearing employing light oil as a lubricant the maximum temperature rise of the oil passing through the bearing is $0.55 \times 10^{-6} \times P_s$ degrees celsius where supply pressure units are MPa . For a high-speed bearing, $K = 9$, the temperature rise is increased by a factor of 10 compared to zero speed. For a supply pressure of 1 MPa, the high-speed bearing has a maximum temperature rise per pass equal to 5.5 °C.

4.6 Flowrate

Concentric flow can be calculated based on a 1-dimensional (1D) solution [3]:

$$q = \frac{\pi \beta P_s h_0^3 \sin \alpha}{6\eta} \left(\frac{1}{\ln D/D_3} + \frac{1}{\ln D_2/D_1} \right) \quad (10)$$

Where, D is the large-end bearing diameter and:

$D_1 = D(1 - 2 \cdot \tan \alpha \cdot L/D)$ is the small-end bearing diameter.

$D_2 = D(1 + 2 \cdot \tan \alpha \cdot a/L \cdot L/D)$ is the small recess diameter.

$D_3 = D(1 - 2 \cdot \tan \alpha \cdot a/L \cdot L/D)$ is the large recess diameter.

A 1D flow solution gives a reasonable estimate for circumferentially wide recesses and large a/L values. However, for circumferentially thin recesses and small a/L values, it is necessary to employ a 2D solution for concentric flow or a 3D solution for eccentric flow. Computed flow can be expressed economically as a dimensionless flow factor:

$$Q_f = \frac{q\eta}{P_s h_0^3} \cdot \frac{a}{L} \cdot \frac{L}{D} \cdot \frac{1}{\beta} \quad (11)$$

1D concentric flow solutions using equation (10) are the same for 3 or 4-recess bearings.

The flow through each restrictor is given by q/n .

5 RESULTS

5.1 Hydrostatic Performance at Zero-Speed

Figure 3 shows pressure contours for a conventional conical hydrostatic bearing having four large recesses running at zero speed, where $L/D = 1.0$ and the semi-cone angle is $\alpha = 15^\circ$. The radial eccentricity ratio is $\epsilon = 0.5$ and the axial position ratio is $\bar{X} = 1.0$. The bearing

geometry is defined by the inter-recess angle $\theta = 30^\circ$ giving a recess angle of 60° . The axial landwidth ratio $a/L = 0.25$. It is seen that pressure is maximum in the heavily loaded recesses and minimum in the lightly loaded recesses on the opposite side. The pressure drops down slightly between the recesses and drops down sharply from the ends of the recesses. For clarity, pressures are only shown for the large end of the bearing. Pressures at the small end are almost similar.

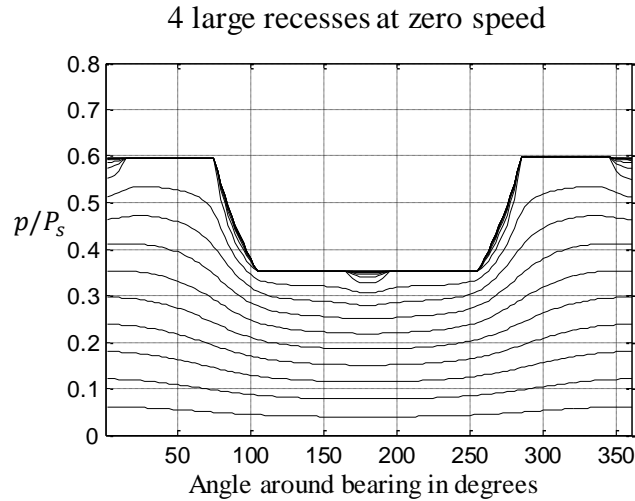


Figure 3. Pressures: $n = 4$, $L/D = 1$, $\frac{a}{L} = 0.25$, $\alpha = 15^\circ$, $\beta = 0.5$, $\epsilon = 0.5$, $\bar{X} = 1.0$, $\theta = 30^\circ$, $\phi = 0^\circ$, $K = 0$

Figure 4 shows the load support at zero speed for the same large recess bearing. Zero speed corresponds to a power ratio $K = 0$. Data are provided for a range of axial position ratios varying from $\bar{X} = 0.5$ to 1.5 . It is seen that axial load support falls away rapidly at $\bar{X} > 1.5$. Radial load support falls away at both extremes. It was found that reducing landwidth in the axial direction to $a/L = 0.1$ gives almost one-third increase in radial load capacity compared with $a/L = 0.25$ so the reduced value was adopted for further development. A further development was to employ 3 recesses instead of 4 which is favourable for radial load support. The aim was to show how load support may be enhanced at higher speeds. Development centred on increasing inter-recess lands to increase area where hydrodynamic pressure can be generated while reducing axial land width ratio to $a/L = 0.1$. A large inter-recess land also has the merit that it reduces inter-recess flows which detract from radial load support. A small axial land width ratio has the merit of spreading recess pressure over the maximum bearing length possible.

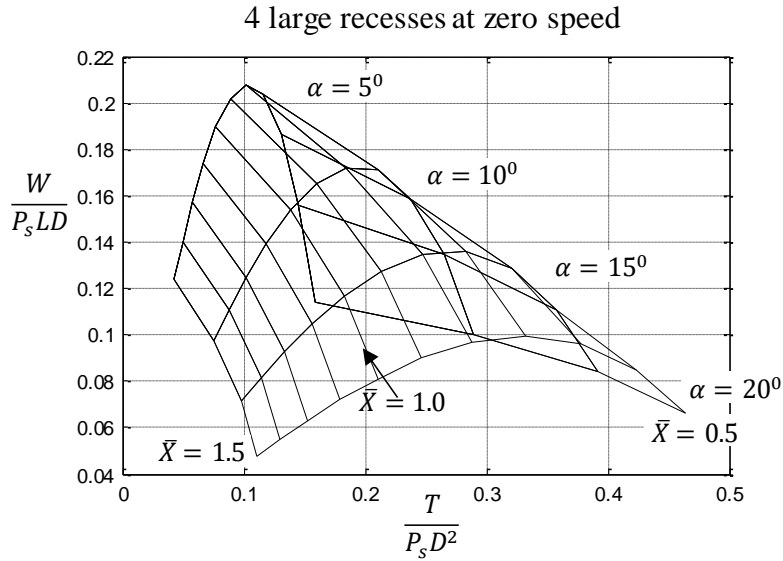


Figure 4. Load support: $n = 4$, $L/D = 1.0$, $a/L = 0.25$, $\beta = 0.5$, $\epsilon = 0.5$, $\theta = 30^\circ$, $\phi = 0^\circ$, $K = 0$
 Figure 5 demonstrates that these changes provide adequate load support even at zero-speed. Figure 5 is for the developed geometry with 3 thin recesses. Combining reduced axial land width $a/L = 0.1$ and very large inter-recess land width, $\theta = 112^\circ$, corresponds to long thin recesses of 8° width. The resulting load support may be compared with Figure 4 for the conventional 4-recess bearing. It shows that zero speed load support is comparable for the two bearings.

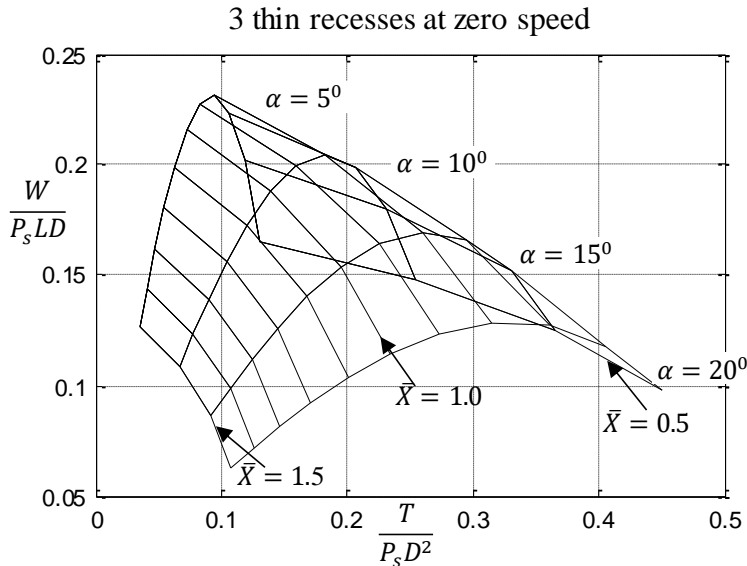


Figure 5. Load support. $n = 3$, $L/D = 1.0$, $a/L = 0.1$, $\beta = 0.5$, $\epsilon = 0.5$, $\theta = 112^\circ$, $\phi = 0^\circ$, $K = 0$
 Since long thin recesses were so successful for the 3-recess bearing, a similar change was tried for a 4-recess bearing where the recess angle was reduced to 5° . Figure 6 shows similarly favourable results. A recess angle of 10° yields almost similar results but the smaller recess angle offers a larger hydrodynamic load support at high speeds.

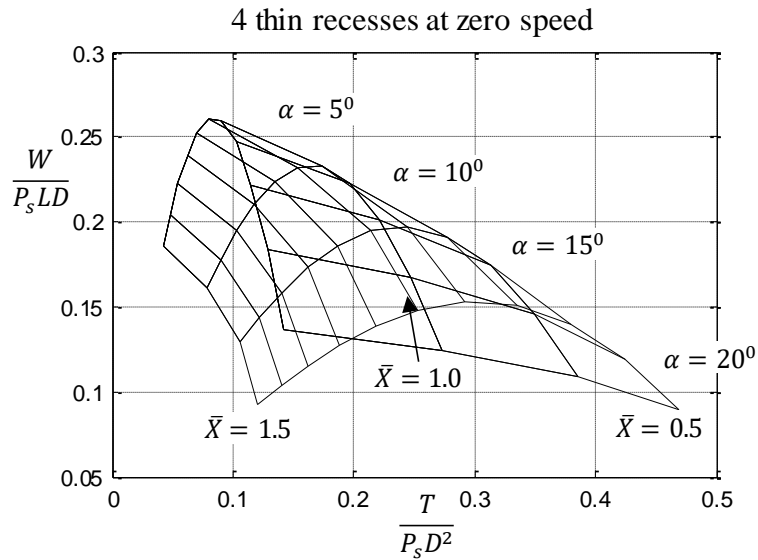


Figure 6. Load support. $n = 4$, $L/D = 1.0$, $a/L = 0.1$, $\beta = 0.5$, $\epsilon = 0.5$, $\theta = 85^\circ$, $\phi = 0^\circ$, $K = 0$

5.2 Hybrid Performance at Low to Moderate Speeds

The optimum power ratio K for purely hydrostatic load support lies in the range 1 to 3. The higher power ratio represents a speed 9 times higher than the lower value. The value $K = 3$ therefore represents a large increase in speed. However, it may still be considered a moderate speed bearing since many hydrodynamic bearings operate with very low pressures and high speeds which lead to much higher power ratios. The following example is given for the maximum of the low to moderate speed range where $K = 3$. Figure 7 shows pressures for the 3-recess bearing. Recess pressures and land pressures are increased in the converging film region while in the diverging film region pressures are reduced. An advantage of design within the power ratio range $1 < K < 3$ is that temperature rise is more moderate than at higher power ratios.

Although pressures are not shown for the 4-recess bearing for the moderate speed condition, the maximum pressure supporting the load was found to be nearly 10% higher for the 3-recess bearing than for the 4-recess bearing.

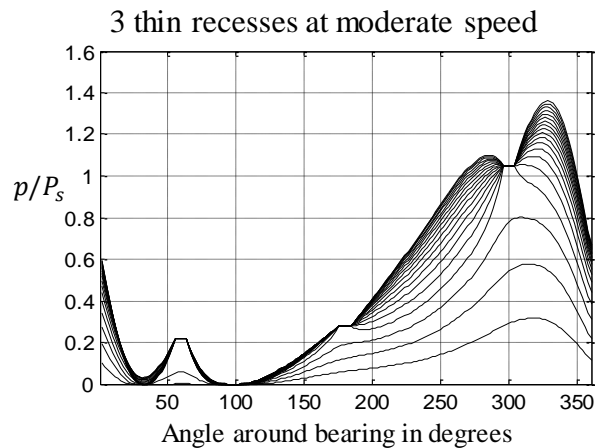


Figure 7. Pressures: $n = 3$, $L/D = 1$, $a/L = 0.1$, $\alpha = 15^\circ$, $\beta = 0.5$, $\epsilon = 0.5$, $\bar{X} = 1.0$, $\theta = 112^\circ$, $\phi = 0^\circ$, $K = 3$

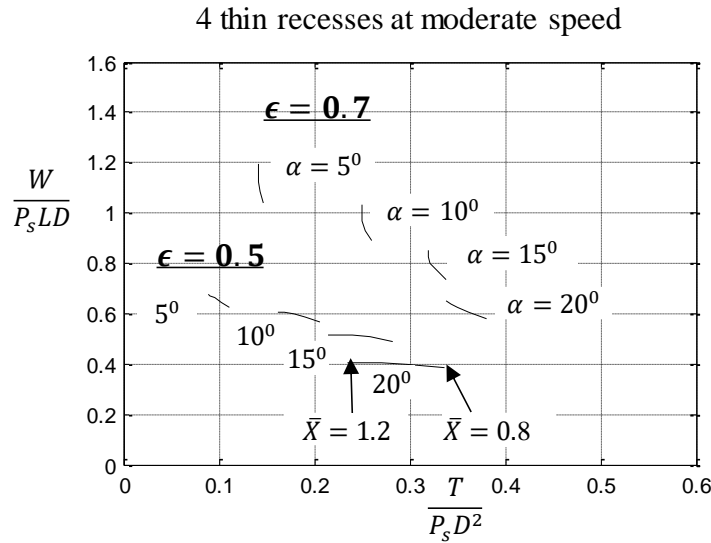


Figure 8. Loads & ϵ : $n = 4$, $L/D = 1.0$, $a/L = 0.1$, $\beta = 0.5$, $\theta = 85^\circ$, $\phi = 0^\circ$, $K = 3$

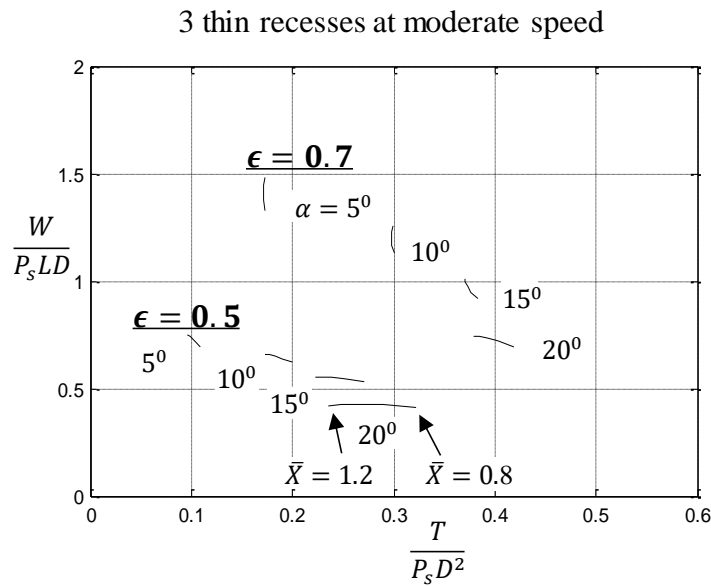


Figure 9. Loads & ϵ : $n = 3$, $L/D = 1.0$, $a/L = 0.1$, $\beta = 0.5$, $\theta = 112^\circ$, $\phi = 0^\circ$, $K = 3$

Figure 8 and 9 show bearing support loads for the two hybrid bearings for $K = 3$. The axial position range for each bearing has been restricted to the range $0.8 < \bar{X} < 1.2$. This allows larger values of radial eccentricity ratio to be safely employed. In this figure two sets of values are shown for $\epsilon = 0.5$ and $\epsilon = 0.7$. Figure 8 shows that bearing load support with long thin recesses is substantially increased at moderate speed compared with zero speed and wide recesses. It is also seen that radial load support increases greatly with radial eccentricity ratio due to hydrodynamic pressures. Load support for the 3-recess bearing is even higher. And, in fact, the increase in load support for both bearings compared to zero-speed load support is more than 100% at the smaller eccentricity ratio and even more at the higher eccentricity ratio.

3 thin recesses at moderate speed

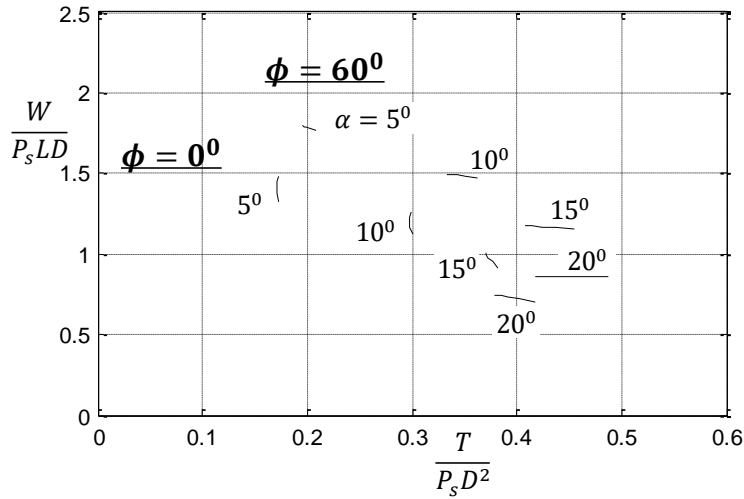


Figure 10. Effect of ϕ : $n = 3, L/D = 1.0, a/L = 0.1, \beta = 0.5, \theta = 112^\circ, \epsilon = 0.7, 0.8 < \bar{X} < 1.2, K = 3$

Figure 10 compares the effect of directing the radial eccentricity towards the middle of the inter-recess land $\phi = 0^\circ$ and the effect of directing the radial eccentricity towards a recess $\phi = 60^\circ$ for the 3-recess bearing. Directing the eccentricity towards the recess yields higher radial load support. Previous figures were presented for the conservative case where $\phi = 0^\circ$. In practice, the direction of the line of eccentricity is usually unknown at the design stage. The attitude angle ψ between the direction of the applied load and the line of eccentricity varies both with eccentricity ratio and with power ratio as shown in Figure 11. For a large inter-recess land, $\theta = 112^\circ$ and very low speed, $K = 0.1$, the attitude angle is less than 40° throughout the range of eccentricity ratios. For high speed, $K = 9$, and small eccentricity ratio, the attitude angle exceeds 80° . At high speed, the shape of the curve is very similar to the well-known case of a purely hydrodynamic bearing, where attitude angle reduces from 90° following an almost a circular arc towards 0° at maximum eccentricity ratio.

Figure 11 also shows a more conventional hydrostatic bearing with 3 large recesses where the inter-recess land $\theta = 40^\circ$. The resulting attitude angle is much smaller even at high speed, $K = 9$, due to the greatly reduced hydrodynamic pressures.

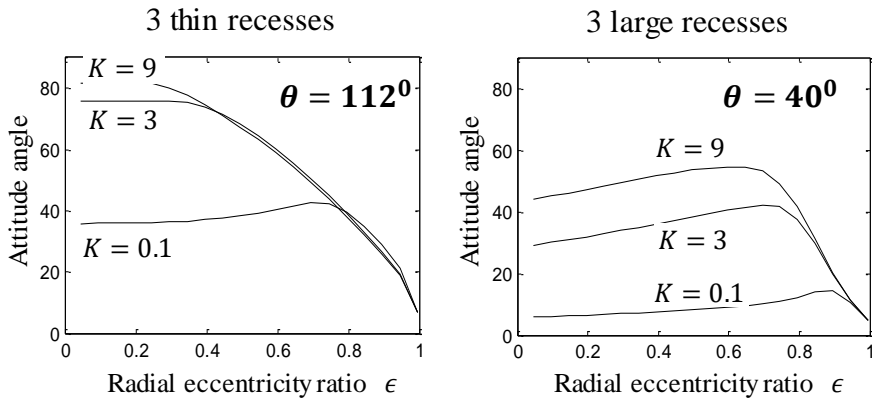


Figure 11. Attitude angle ψ & ϵ : $n = 3, L/D = 1.0, \alpha = 15^\circ, a/L = 0.1, \beta = 0.5, \phi = 0^\circ, \bar{X} = 1$

5.3 Hybrid Performance at High Speed

Previous experimental and theoretical research on conventional recessed hydrostatic journal bearings, showed that hybrid bearings could operate at much higher values of power ratio than $K = 3$, subject to selection of suitable bearing materials and maximum temperature rise, [14]. A new optimization procedure based on minimum total power for total load support included both hydrostatic and hydrodynamic contributions. For plain slot entry designs, values of power ratio up to and exceeding $K = 12$ were employed. One concern arose at extremely high values of power ratio where $K \gg 12$. For double-row slot entry bearings it was necessary to avoid a 'hot spot' in the minimum film thickness region between the two rows of slots. This potential problem arose when there was lack of sufficient oil recirculation at the mid-length position in the bearing [15]. The thin recess designs, however, ensure continuous oil flow through the bearing mid-length zone.

At high speed, $K = 12$, the pressures for an increased eccentricity ratio of 0.7, show that hydrodynamic pressures become even more dominant, Figure 12. The inlet pressures due to the recesses have the beneficial effect of reducing the tendency for cavitation seen in more conventional hydrodynamic bearings. At the 60° angle position around the bearing, positive pressure is provided in the diverging region. This positive pressure moderates the extent of the cavitation.

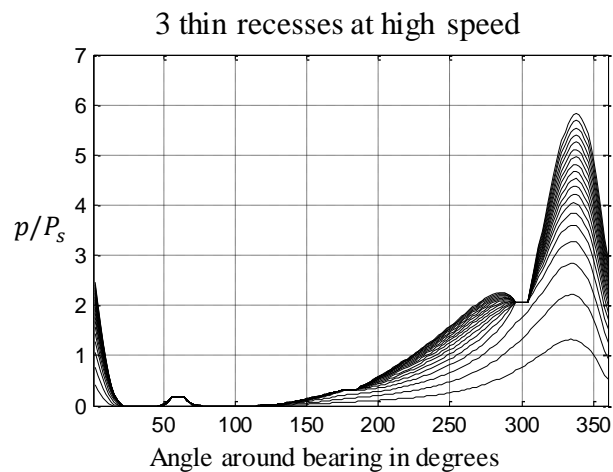


Figure 12. Pressures: $L/D = 1$, $a/L = 0.1$, $\alpha = 15^\circ$, $\beta = 0.5$, $\epsilon = 0.5$, $\bar{X} = 1.0$, $\theta = 112$, $\phi = 0^\circ$, $K = 12$

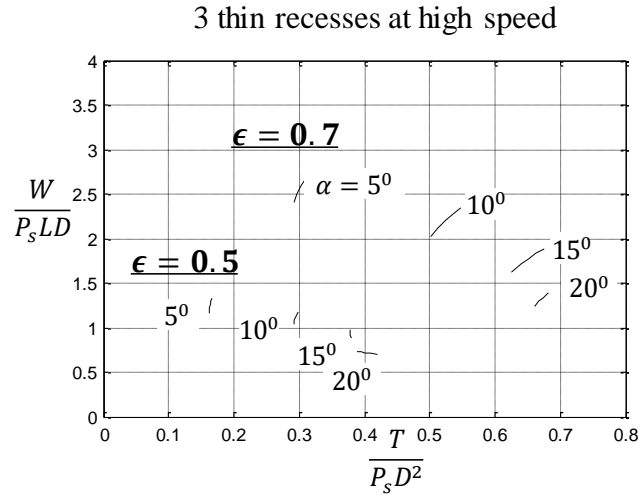


Figure 13. Loads: $n = 3$, $L/D = 1.0$, $a/L = 0.1$, $\beta = 0.5$, $\theta = 112^\circ$, $\phi = 0^\circ$, $0.8 < \bar{X} < 1.2$, $K = 12$

Figure 13 for the 3-recess bearing at high-speed compared with Figure 6 for the conventional zero-speed 4-recess bearing, shows that radial load support is almost quadrupled at $\epsilon = 0.5$. Load support is almost doubled compared with the moderate speed case, $K = 3$, shown in Figure 9. Compared to the zero speed designs, at high speed and $\epsilon = 0.7$, load support is increased by an order of magnitude. The results confirm the benefits of increased load support employing long thin recesses. Figure 14 for the equivalent 4-recess case yields rather lower loads than the 3-recess case but the benefits are also substantial.

For even higher values of power ratio, where $K > 12$, there are diminishing returns supporting a finding by Koshal and Rowe who minimized the function load/power, [14]. It was found for slot-entry bearings that optimum power ratio for hybrid operation lies within the range $9 < K < 12$.

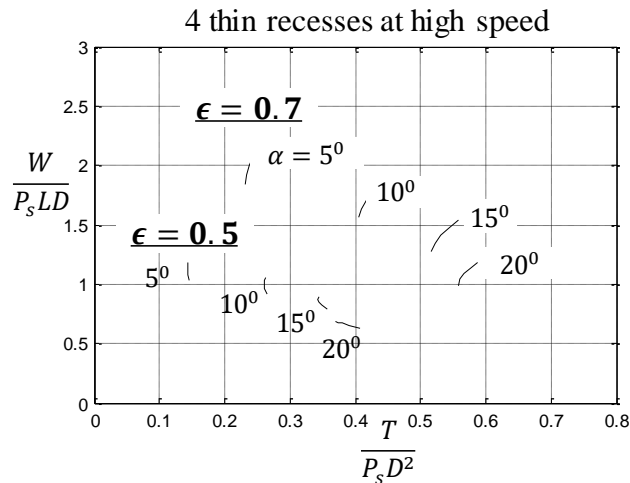


Figure 14. Loads: $n = 4$, $L/D = 1.0$, $a/L = 0.1$, $\beta = 0.5$, $\theta = 85^\circ$, $\phi = 0^\circ$, $0.8 < \bar{X} < 1.2$, $K = 12$

Load support varies significantly depending on the eccentricity ratio, and also on the position of the recesses relative to the direction of the applied loads, as seen in Figures 10 and 11. Figure 14 shows that the difference between the minimum radial load support and the maximum radial load support is almost 80% at an eccentricity ratio $\epsilon = 0.7$. As a rough and easily remembered

guide for design of journal bearings, the mid-land position between the recesses should roughly lie so as to oppose the direction of the applied loads on the bearing. From Figure 15, the maximum load support is when ϕ is slightly greater than 40° , which results in a recess approximately 15° inside the diverging film region and the applied load favorably directed towards the maximum pressures in the converging film region.

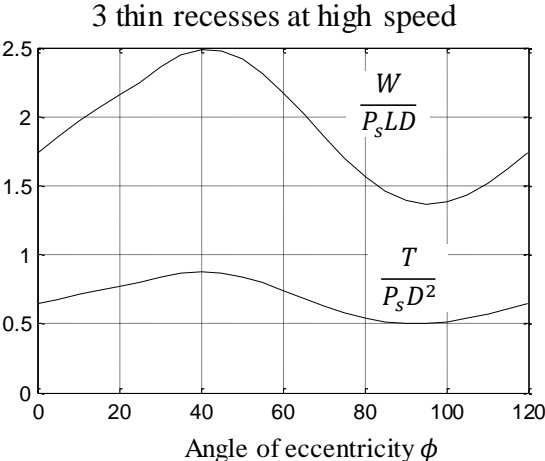


Figure 15. Load support with ϕ : $n = 3$, $L/D = 1.0$, $\alpha = 15^\circ$, $a/L = 0.1$, $\beta = 0.5$, $\theta = 112^\circ$, $\bar{X} = 1$, $\epsilon = 0.7$, $K = 12$

5.4 Load Support for Complementary-Cone Arrangements

Two complementary-cone arrangements are shown schematically in Figure 2, where two conical bearings provide axial thrust loads acting in opposition. Complementary cone arrangements are convenient for spindles that have to support overhung loads as shown. The more centrally located bearing nearest the overhung load experiences the maximum radial load. The two conical bearings must be well separated so as to avoid excessive misalignment of the journal and bearings under the action of radial loads. Maximum radial load on the front bearing has to be supported based on the data provided in the above figures for a single cone bearing. However, the maximum axial load depends on the resultant axial support load for the two bearings acting in combination. With zero externally applied load, the resultant axial thrust due to the two bearings is therefore zero and the resultant axial thrust loads are much reduced compared to the thrust loads for a single pad in the range $0.8 < \bar{X} < 1.2$. Indicative data for design of a limited range of complementary conical bearings is therefore presented on the basis of radial support load for a single bearing and axial support load for two opposed bearings. Examples are shown in Figures 16-17 for a range of speeds and L/D ratios.

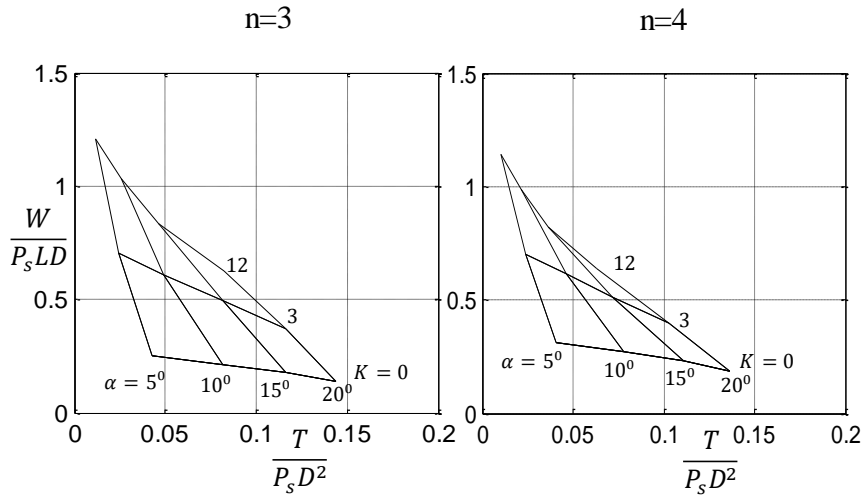


Figure 16. Thin recess complementary cones: $L/D = 1.0, a/L = 0.1, \beta = 0.5, \bar{X}_1 = 0.8, \bar{X}_1 = 1.2, \epsilon = 0.5$.

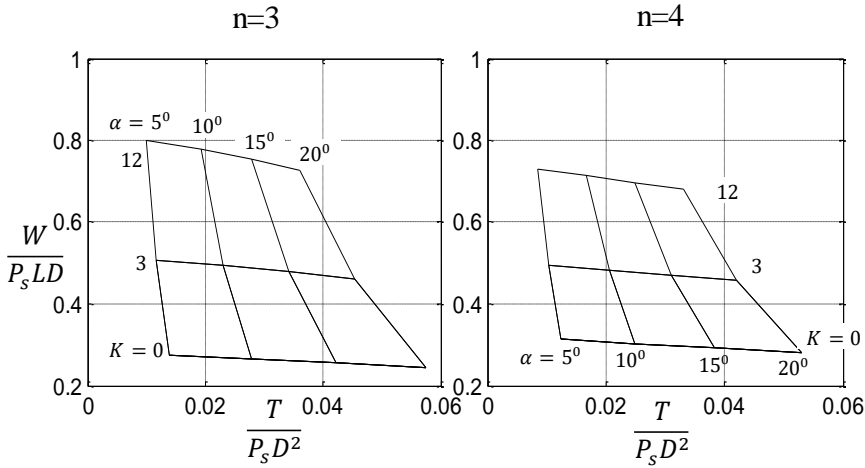


Figure 17. Thin recess complementary cones: $L/D = 0.5, a/L = 0.1, \beta = 0.5, \bar{X}_1 = 0.8, \bar{X}_1 = 1.2, \epsilon = 0.5$.

It can be seen that radial loads increase at the higher speeds corresponding to $K = 3$ and $K = 12$ compared with zero speed with $K = 0$, but, axial loads are reduced with increasing speeds. This tends to reduce the range of operating speeds that can reasonably be employed. A reasonable maximum speed for operation corresponds to a power ratio, $K = 12$.

While 3-recess arrangements give slightly more load support than 4-recess arrangements the difference is modest. Reducing the L/D ratio from 1 to 0.5 has the effect of reducing radial and axial loads.

5.5 Flowrate and Flow Factors

The main variables for the flow factor are the L/D ratio and the semi-cone angle α as illustrated in Figure 18. Flow factors based on the 1D solution are a reasonable estimate for bearings having 3 or more wide recesses.

Flow factors are reduced in the 2D results due to pressure drop between the recesses and also to some extent due to eccentricity ratio. Figure 18 also gives concentric flow factors based on the accurate 2D solution for 3 thin recesses with $\theta = 112^\circ$ and $a/L = 0.1$. The flow factor values are very similar for 4 thin recesses with $\theta = 85^\circ$ and $a/L = 0.1$

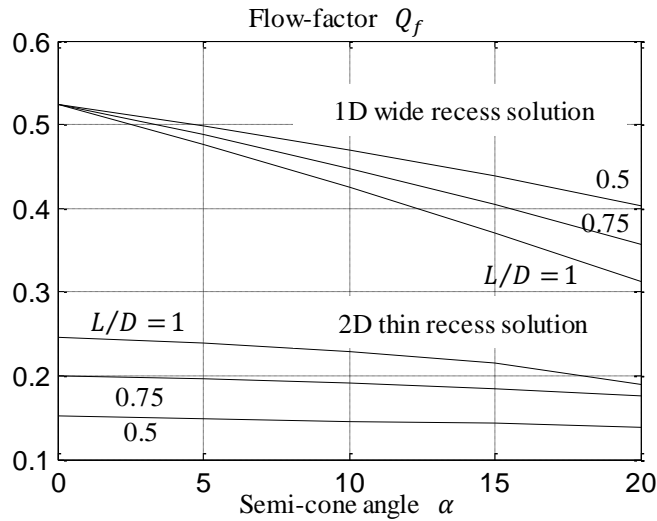


Figure 18. Concentric flow from 1D wide recess solution compared with accurate 2D thin recess solution: $\theta = 112^\circ$, $n = 3$, or $\theta = 85^\circ$, $n = 4$ and $a/L = 0.1$.

The flow factors for 3 and 4 recess bearings are increased as axial land width is increased, whereas actual values of flowrate q are reduced. This difference is a consequence of the definition of flow factor Q_f . The flow factors shown in Figure 19 are for $a/L = 0.25$. Figures 18 and 19 illustrate the range of values likely to apply in practice.

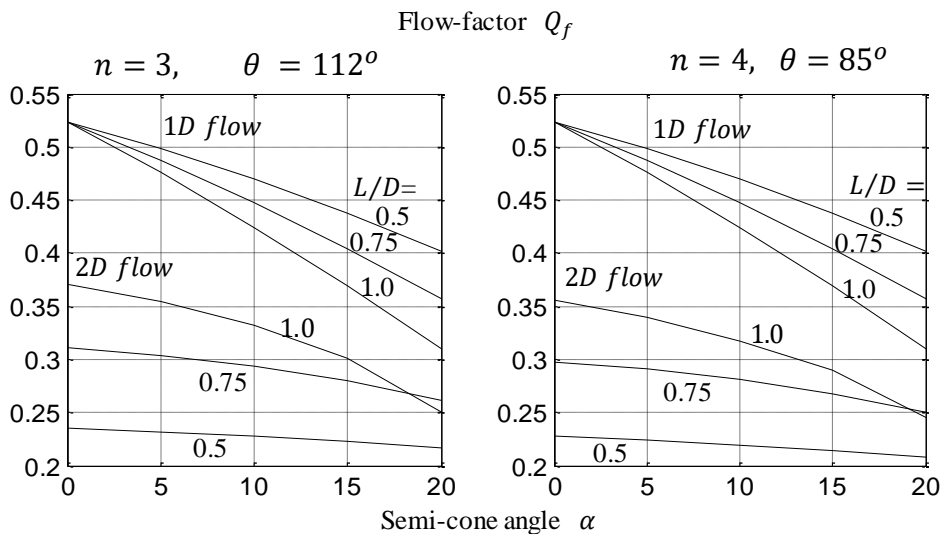


Figure 19. Concentric flow from 1D solution compared with accurate 2D thin recess solution: $\theta = 112^\circ$, $n = 3$ or $\theta = 85^\circ$, $n = 4$ and $a/L = 0.25$.

5 CONCLUSIONS

For high speeds, recessed conical hydrostatic bearings benefit from long and thin recesses as opposed to low speed bearings where wide recesses are usually employed. Three and four recess bearings employing long and thin recesses perform well throughout the speed range from zero speed to high speed.

Speed ranges can be conveniently defined by employing power ratio in the design process. Bearings operating in the range $K = 9$ to 12 are high speed bearings. Operation with $K > 12$

is not recommended due to diminishing returns in terms of load supported for power expended. High power ratios also lead to higher values of temperature rise.

Data provided reveal the benefits for radial load support from operating at high speeds.

6 REFERENCES

1. Rowe WB. Experience with four types of grinding machine spindles. *Proceedings of 8th Int. MTDR Conference*, held at the University of Manchester, Pergamon Press, Oxford, London, 1967, pp 453-477.
2. Mason PA. A new profile forming machine. CNAA PhD thesis, Lanchester Polytechnic, now Coventry University, Coventry. August 1973.
3. Stansfield FM, *Hydrostatic bearings, Chapter 12*. Machinery Publishing Company, UK, 1970.
4. Aston RL et al. Design of conical hydrostatic journal bearings. *Machinery and Production Engineering*, 18 Feb 1970, 116, 2988, pp 250-254.
5. Aston RL et al. Hydrostatic bearings for combined radial and axial thrust applications. *Externally Pressurized Bearings Conference*, Paper C28, pp 228-244, Proc. Instn. Mech. Engrs, London, UK, 1971.
6. Ettles C and Svoboda O. The application of double conical journal bearings in high speed centrifugal pumps. *Proc. Instn. Mech. Engrs, London*, 1975, 189, 38/75, pp 221-230.
7. Rowe WB. *Hydrostatic and Hybrid Bearing Design, Chapter 12*. Butterworths, London, UK. 1983.
8. Sharma et al. Performance analysis of a multi-recess capillary compensated conical hydrostatic journal bearing. *Tribology International*. 2011, 44, 617-626.
9. Rowe WB. *Hydrostatic, Aerostatic and Hybrid Bearing Design*. Butterworth Heinemann/Elsevier Press, Oxford, UK. 2012.
10. Zuo X et al. Design and parameter study of a self-compensating hydrostatic rotary bearing. *International Journal of Rotating Machinery*, 2013. Article ID 638193, 10 pages. Hindawi Publishing Corporation.
11. Khakse PG et al. Comparative performance of a non-recessed hole-entry hybrid/hydrostatic conical journal bearing compensated with capillary and orifice restrictors. *Tribology in Industry*. 2016, 38, 2, 133-148.
12. Bassani R and Piccigallo B. *Hydrostatic Lubrication*. Tribology Series, v22, 1-542. Elsevier.
13. Opitz H. Pressure Pad Bearings. *Conference on Lubrication and Wear, Fundamentals and Applications to Design*. Proc. Instn. Mech. Engrs, London, UK, 1967, 182(Part 3A), pp 100-115.
14. Rowe WB and Koshal D. A New Basis for the Optimization of Hybrid Journal Bearings. *Wear*, 1979, 64, 1, pp 115-131.
15. Ives D and Rowe WB. The Effect of Multiple Supply Sources on the Performance of Heavily Loaded Pressurized High-Speed Journal Bearings. *Tribology Convention*, 1-3rd July, 1987, Proc. Instn. of Mech. Engrs, London, UK.